Numerical Continuation for a Diblock Copolymer Model in One Dimension

Ian Johnson

May 24, 2011

Abstract

Diblock copolymers are a class of materials formed by the reaction of two linear polymers. The different structures taken on by these polymers grant them special properties, which can prove useful in applications such as development of new adhesives and asphalt additives. The diblock copolymer equation governs the formation of these polymers. Using the software package AUTO, continuation analysis of the equilibria of the diblock copolymer equation in one dimension was performed. The results of simulations and continuation are synthesized.

1 Introduction

Diblock copolymers are formed by the chemical reaction of two linear polymers, or blocks, which contain different monomers. These blocks may often be thermodynamically incompatible, which means that following the reaction the blocks may be compelled to separate. However, following the reaction the blocks are already covalently bonded. This means that it is not possible for them to separate on a macroscopic scale without adopting an entropically unfavorable extended configuration, in which the number of available states is severely limited relative to the native configuration. This conflict causes a phenomenon called **microphase separation**, where the two blocks separate on a mesoscopic scale. Microphase separation grants diblock copolymers the capacity for self-assembly into special geometries. These allow for the creation of materials with designer physical properties.

A model has been developed for microphase separation in diblock copolymers. The model, in the form that is used here, is as follows:

$$\begin{aligned} u_t &= -\Delta(\Delta u + \lambda(u - u^3)) - \lambda\sigma(u - \mu) \\ \mu &= \int_\Omega u(x)\,dx \\ \frac{\partial u}{\partial n} &= \frac{\partial \Delta u}{\partial n} = 0, x \in \partial\Omega \end{aligned} \tag{1}$$

The function u tracks the density of the two components across the domain, with the value 1 being interpreted as only component A being present at a point, and the value -1 being interpreted as only component B being present at a point. There are also three varying parameters, λ, σ, and μ, which have physical meanings. λ and σ are dimensionless functions of material parameters defined as follows:

$$\lambda = \frac{3\frac{N_A}{N}(1 - \frac{N_A}{N})\chi|\Omega|^{2/3}}{l^2}$$
$$\sigma = \frac{36|\Omega|^{2/3}}{(\frac{N_A}{N})^2(1 - \frac{N_A}{N})^2 l^2 \chi N^2},$$

where N_A is the number of A units in the chain, N is the total length of the chain, χ is the Flory-Huggins interaction parameter which describes the strength of the repulsion, $|\Omega|$ is the (physical) size of the domain,

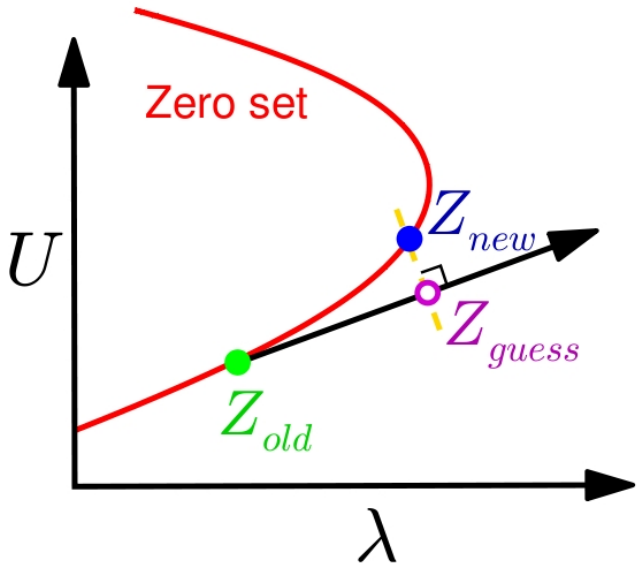

Figure 1: A schematic of the numerical continuation procedure. The "zero set" is the set of points where the function defining the time derivative in (1) is zero; see Section 2.3
.

and l is the Kuhn statistical length which essentially measures typical distances between monomers. Informally, λ being large represents the short range repulsions being strong, inducing a strong compulsion to separate, while σ being large represents the long range chain elasticity forces being strong, inducing a strong compulsion to hold together.

This work focuses on this model in one dimension, in which case the model reduces to:

$$\begin{aligned} u_t &= -(u_{xx} + \lambda(u - u^3))_{xx} - \lambda\sigma(u - \mu) \\ \mu &= \int_0^1 u(x)\,dx \\ u_x &= u_{xxx} = 0, x = 0, 1. \end{aligned}$$

Past work on this model has primarily used direct numerical simulation. Some difficulties present themselves when doing so, however, including metastability concerns. In general methods must be used to overcome this metastability if true long-term behavior is to be studied, and even when this is done the computational time becomes large.

This work uses a method that is new to this problem called numerical continuation. In this method, the equilibrium problem is considered as parameters vary. The method proceeds essentially by beginning at an initial equilibrium, estimating the next equilibrium at a new parameter value. A correction step is then performed to arrive at a new equilibrium, which seeds the method in the next step, eventually arriving at a whole family of equilibria at a variety of parameter values. This is summarized schematically in Figure 1.

This is described in detail in the Methods section. This method is implemented in the software package called AUTO, which also implements bifurcation detection methods. These methods can be used in combination to develop a full bifurcation diagram. Figure 2 shows a typical bifurcation diagram.

This bifurcation diagram can be used to determine properties of the time-varying equation. For example, at each equilibrium, stability computation can be performed. In doing so, the (possible) time-invariant long-term behavior(s) for a given set of parameter values can be seen directly, since these will be exactly the stable equilibria. This is particularly useful for this problem, because it is expected that the long-term behaviors will be exactly the time-invariant long-term behaviors. This is in part because the dissipative

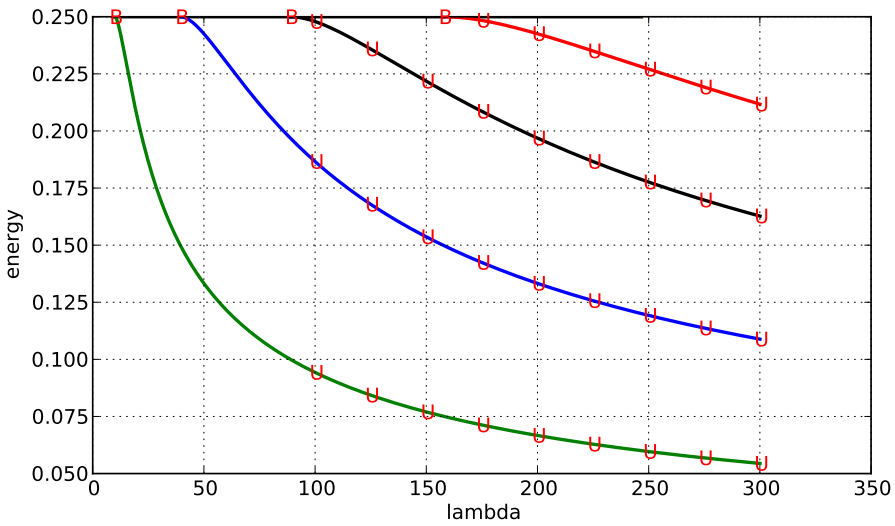

Figure 2: A typical bifurcation diagram with $\sigma = \mu = 0$. The horizontal axis is λ; the vertical axis is an energy functional of the problem.

character of the equation prevents periodic solutions.

As parameters vary, the exact position of changes in stability can be observed; in fact, these will always occur at bifurcation points, which can be proven using the Implicit Function Theorem. In fact, with a modified two parameter continuation method, this reasoning can be used to draw stability boundaries in, for example, the (σ, λ), boundary, creating a diagram which resembles a phase diagram; this method is also developed in this work.

Numerical continuation is combined with direct numerical simulation in this work. One critical use of this is to determine how qualitative changes occur as parameters vary. For example, while an equilibrium may become stable at a particular set of parameter values, the behavior in a small neighborhood of those parameter values is also of interest. Perhaps, for example, the movement away from that equilibrium takes longer and longer before it eventually stops happening altogether. There is no obvious way to reveal this information with numerical continuation being applied to the equilibrium equation. On the other hand, continuation can reveal these regions where simulation may reveal critical information, and so the methods complement each other closely.

2 Methods

There are three primary methods used in this work: numerical continuation in one and two parameters, and direct simulation. Numerical continuation in one parameter is used to compute the bifurcation structure of the problem. The parameter varied in one parameter continuation is always λ; this is essentially because the objective is to look at how the λ-varying structure varies as σ varies. In addition, a stability computation is performed at each equilibrium point computed. Numerical continuation in two parameters is used to follow the location of specific bifurcations observed in the one parameter case in the (σ, λ) plane. This is desirable because it may be difficult to repeatedly find the bifurcations with one parameter continuation if they become farther and farther away from a known, "simple" equilibrium. Finally direct simulation is used to obtain any information that cannot be readily attained via numerical continuation.

2.1 Discretization

All of these different methods require a discretization of the equation. This discretization is done using a Fourier series approximation. This is motivated by the fact that the only differential operator in the equation is the Laplacian, whose eigenfunctions on this domain with these boundary conditions are very easy to find:

$$\varphi_k = \cos(k\pi x), k \in \mathbb{N} \cup \{0\}.$$

It is then expected from spectral theory that a Fourier series of a smooth solution to an equation like this should converge to the correct solution and do so very quickly, exponentially fast in N in fact. That is:

$$u(x) = \sum_{k=0}^{\infty} a_k \cos(k\pi x) \approx \sum_{k=0}^{N} a_k \cos(k\pi x)$$

for a relatively small N. In most of this work N=60 was sufficient. In the context of spectral methods, "sufficient" means that the coefficients of the modes whose frequency is near N are very small relative to the others, the idea being that the modes of even higher frequency will generally be even smaller and thus can be reasonably discarded. Here "very small" means that they are at most 10^{-6}.

Much of the computational aspect of the problem is simplified by using this discretization. In particular, the operation of computing the second derivative reduces to multiplying the vector of Fourier coefficients by a diagonal matrix, since the entries of this vector are coefficients of the cosines. That is, if:

$$u = \sum_{k=0}^{N} a_k \cos(k\pi x)$$

then:

$$u'' = \sum_{k=1}^{N} -k^2\pi^2 a_k \cos(k\pi x)$$

and so the coefficients a_k are each multiplied by $-k^2\pi^2$. The discretization also does not need to be as fine as, for example, a finite difference method. However, the operation of computing the nonlinearity is made more complicated, because there is no simple function relating the Fourier coefficients of a function to the Fourier coefficients of the cube of that function. However, a Galerkin method can be used to compute the nonlinearity. By computing at least 3N function values, the Fourier coefficients of this particular nonlinearity can be computed exactly. This is because:

$$\begin{aligned} u^3 &= \left(\sum_{k=0}^{N} a_k \cos(k\pi x)\right)^3 \\ &= \sum_{i=0}^{N}\sum_{j=0}^{N}\sum_{k=0}^{N} a_i a_j a_k \cos(i\pi x)\cos(j\pi x)\cos(k\pi x) \\ &= \sum_{i,j,k} \frac{1}{4} a_i a_j a_k \left(\cos((i-j-k)\pi x) + \cos((i+j-k)\pi x) + \cos((i-j+k)\pi x) + \cos((i+j+k)\pi x)\right) \end{aligned}$$

using the product-to-sum identities from trigonometry. Then the highest frequency term in this sum is the $\cos(3N\pi x)$ term. In practice the vector is then truncated back to length N, resulting in a good approximation of the nonlinearity.

Computationally speaking, the Fourier transforms necessary to do this analysis were performed by FFTW's discrete cosine transform in this work, which can be called directly from the user-provided function file in AUTO.

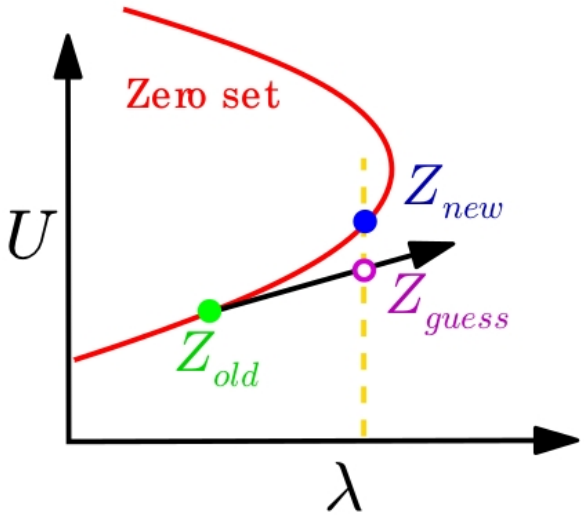

Figure 3: Schematic of "natural" continuation. Note that here Z_{new} is above Z_{guess}, and so the method continues; within a few iterations, however, Z_{guess} will be to the right of the zero set, and the method will fail.

2.2 Continuation

The numerical continuation procedure begins with a known equilibrium at a given set of parameter values. From there, it makes a perturbation in one parameter without varying anything else. This is necessary because there are not two points to use to approximate a tangent direction. In AUTO, at this stage a Broyden method is performed to correct the perturbation and return it to an equilibrium point. Now there is a tangent direction available, and perturbations are made in this tangent direction at each subsequent stage. Correction steps are then made, and so this method falls into the class of predictor-corrector methods.

The correction step is somewhat subtle. The reason for this is that we do not have a Jacobian for the n+1 dimensional system involving both the parameter being varied and the equilibrium point to be found. That is, we only automatically have n equations in n+1 unknowns, and so we cannot find a unique solution. The answer is to produce another equation, but the best choice is not immediately obvious.

The immediately obvious choice is to freeze the parameter. This results in the so-called "natural" continuation method, depicted schematically in Figure 3, and it works fairly well in many cases. It runs into a problem, however, when the curve "turns around" in the space, which can and does happen in practice. In short, when this happens, eventually the natural continuation method will reach a parameter value where the branch it is currently on does not exist. In this case it may simply not converge, or it may find a new branch entirely. In either case it will not make its way to the other side of the curve.

The solution to this issue is called arclength continuation, depicted schematically in Figure 3. In arclength continuation, instead of fixing the parameter value, the correction step is done along a direction orthogonal to the original perturbation direction. This does not completely guarantee that convergence will occur; however, it does fix the issue of losing convergence when the curve "turns around". In the context of this problem, using the Fourier discretization described in Section 2.1, the problem reduces to a nonlinear system. Since the second derivative of $\cos(k\pi x)$ is $-k^2\pi^2\cos(k\pi x)$, each equation of the system is of the form:

$$0 = -k^4\pi^4\hat{u}_k + \lambda k^2\pi^2\left(\widehat{u-u^3}\right)_k - \lambda\sigma\hat{u}_k$$

for $k = 1 \ldots N$. Thus we are attempting to find the "zero set" of this function, that is the set of vectors such that this function is zero; this explains the notation of Figure 1 and Figure 3.

In this form, solving the nonlinear system turns out to be numerically infeasible. The reason for this is that the matrix that results from using this form directly is very badly scaled. However, if each of these equations is divided by a constant, the solution set will not change; any solution to the rescaled equation would be a solution to the original equation and vice versa. Consequently the equation is rewritten in the form:

$$0 = -\hat{u}_k + \frac{\lambda\left(\widehat{u-u^3}\right)_k}{k^2\pi^2} - \frac{\lambda\sigma\hat{u}_k}{k^4\pi^4}$$

and in this form solving the system has been numerically feasible. This has repercussions elsewhere, such as in the stability computation; see Section 2.4.

2.3 Using AUTO

From the standpoint of using AUTO to perform this method, essentially all that must be done is the specification of a collection of constants, including the initial equilibrium itself as well as a variety of numerical parameters, of which the most important are probably the step size parameters DS (the initial step size, which is also the size of the first step from any bifurcation point), DSMIN (the minimum step size the program will use before terminating and assuming convergence has failed), and DSMAX (the maximum step size the program will use before no longer increasing the step size). These are quite problem-dependent; for example, in some cases making these too large will cause bifurcations to be missed, while in other cases making these too small will "trap" the method close to a bifurcation point, instead of correctly following the curves coming out of it.

The other main parameters that are important are the number of modes used, NDIM, and the tolerances for convergence and bifurcation detection. The number of modes generally must increase as the coefficient of the nonlinearity λ increases. The convergence and bifurcation detection tolerances usually can remain fixed, with occasional exceptions when a particular bifurcation proves especially difficult to find reliably.

Two parameter continuation is built into AUTO as well. In two parameter systems, for certain classes of bifurcation points, as well as certain, sufficiently symmetric bifurcation points, AUTO can follow the location of a bifurcation point in two parameters. The latter type appears in this work; in the $\mu = 0$ case, Doing this requires it to be given a bifurcation diagram object, the label of the bifurcation of interest, and the parameter ISW to be set to the value 2. Two parameter continuation is used in this work primarily to follow the location of stability transitions on different branches; see Section 3.4.

2.4 Stability Computation

At each equilibrium point u computed via continuation, stability computation is performed. This is useful for obtaining information about long-term behavior, and in particular for tracking changes in behavior as the model moves away from the Cahn-Hilliard case. The computation is performed by computing the eigenvalues of the approximate Jacobian. The Jacobian is computed as follows.

Begin by linearizing the equation from u in the direction of v. Every term in the equation except $(u^3)_{xx}$ is already linear, and so there is nothing to be done there. $(u^3)_{xx}$ can be linearized as $(3u^2v)_{xx}$. We then have the eigenvalue equation:

$$-v_{xxxx} - \lambda v_{xx} + \lambda(3u^2v)_{xx} - \lambda\sigma(v-\mu) = \Lambda v$$

where Λ is the eigenvalue. It is also required that v be a direction in which the system is permitted to move. This means that it must also satisfy the Neumann boundary conditions, and must satisfy a mass constraint of zero; thus the μ in the equation is in fact 0 in all cases.

Given this, we want to compute the Jacobian of the transformation on the left side. This Jacobian is computed in Fourier space. This makes most of the terms in the Jacobian straightforward to compute. The second derivative operator is simply a diagonal matrix $-K$ whose diagonal entries are the eigenvalues of the Laplacian; that is, $-k^2\pi^2$. Applying another second derivative operator results in a diagonal matrix K^2

whose diagonal entries are the squared eigenvalues of the Laplacian, $k^4\pi^4$. This takes care of most of the terms in the equation, with the exception of the nonlinear term $(3u^2v)_{xx}$.

It may be seen that this function is linear in v. Since v is being represented as a finite linear combination of cosines, this means that for each u there should be a matrix representation of this transformation. This matrix representation is computed in the standard way, by making the columns of the matrix into the output when the transformation is applied to each of the basis vectors. Thus the kth column consists of the Fourier coefficients of $(3u^2 \cos k\pi x)_{xx}$. Given the Fourier coefficients of u, this may be computed without too much difficulty. First map u and $\cos k\pi x$ to real space, and perform the multiplication there to obtain a vector containing values of $3u^2 \cos k\pi x$. Then map back to Fourier space and compute the second derivative as before.

Denoting the operator mapping v to $3u^2v$ by $A(u)$, then, we have that the Jacobian is of the form:

$$J(u) = -K^2 + \lambda K - \lambda K A(u) - \lambda\sigma I$$

where I denotes the identity matrix. Eigenvalues of this matrix may then be computed in order to perform stability computation, with each positive eigenvalue indicating the existence of an unstable direction.

Computationally speaking this stability computation is performed by first manually constructing the matrix inside the AUTO function file, and then calling LAPACK's dgeev solver, also directly from the AUTO function file. The reason it is not done directly using AUTO's stability code is because of the rescaling that was mentioned in Section 2.3, which in principle could modify the eigenvalues and eigenvectors of the "Jacobian" used by AUTO.

2.5 Direct Simulation

Direct simulation is used in combination with numerical continuation in this work. The two methods complement one another closely. For example, numerical continuation may find that there are multiple globally stable equilibria for a given parameter value. Without direct simulation, information about attraction to the different equilibria from different initial conditions is not available. It is even possible that the basins of attraction of some stable equilibria may not contain the initial conditions of interest, which in this context are random, small perturbations from the homogeneous equilibrium. These initial conditions are of interest because these simulate a state which is almost perfectly mixed, which would be typical of a diblock copolymer melt before separation.

On the other hand, direct simulation will also miss certain information. For example, metastability may arise during a simulation. When this occurs, it may appear that a given state is stable, and after a long time that state may eventually disappear. Using direct simulation alone, the simulations might end before the state disappears, and an incorrect conclusion could be drawn. It is also possible for motion to be so slow in the continuous case that it does not even appear in the discretized equation until the discretization becomes much more fine, or in some cases infinitely fine. Numerical continuation can often resolve metastability issues; since normally a metastable state would be near an equilibrium point, stability computation at that equilibrium would show that it was weakly unstable.

The scheme used was developed by Mike Atkins of George Mason University and is as follows:

$$\hat{u}_j^{(k+1)} = \frac{\hat{u}_j^{(k)} + h\lambda\widehat{(u-u^3)}_j^{(k)} K_j}{1 + hK_j^2 + h\lambda\sigma}$$

where the subscripts $j = 1, 2, \ldots N$ index vectors, superscripts denote iterates, hats denote vectors of Fourier coefficients, K is a vector containing eigenvalues of the Laplacian, and h is the step size. N is, as in continuation, generally 60 in this work; h is generally quite small, on the order of 10^{-6} or 10^{-7}; the reason for this is primarily because the motion is quite fast early in a simulation. A dynamic step size could significantly improve the method.

3 Results

There are four sets of results determined. The first are analytical results about the bifurcation structure at the homogeneous equilibrium, where the bifurcation equation reduces to a linear ordinary differential equation with constant coefficients. The second, third and fourth are derived from the numerical methods discussed above: one parameter continuation, direct simulation, and two parameter continuation, respectively.

3.1 Analytical Results

We have analytically determined that the locations of bifurcations from the homogeneous equilibrium are as follows:

$$\lambda(k, \sigma, \mu) = \frac{k^4\pi^4}{k^2\pi^2(1 - 3\mu^2) - \sigma}$$

Proof. Recall the eigenvalue equation from Section 2.4:

$$-v_{xxxx} - \lambda v_{xx} + \lambda(3u^2 v)_{xx} - \lambda\sigma v = \Lambda v$$

where Λ is the eigenvalue, and where the boundary conditions and a mass constraint of zero are forced. Set $\Lambda = 0$ to find bifurcation points. At the homogeneous equilibrium, $u = \mu$ for all x, so the equation reduces to:

$$-v_{xxxx} - \lambda v_{xx} + \lambda 3\mu^2 v_{xx} - \lambda\sigma v = 0$$

This is a fourth order linear homogeneous ordinary differential equation with constant coefficients. Standard boundary value problem methods show that the only nonzero solutions are $v = \cos(k\pi x)$, in which case:

$$-k^4\pi^4\cos(k\pi x) + \lambda k^2\pi^2\cos(k\pi x) - \lambda 3\mu^2 k^2\pi^2\cos(k\pi x) - \lambda\sigma\cos(k\pi x) = 0$$

Dividing through by $\cos(k\pi x)$, we obtain:

$$-k^4\pi^4 + \lambda k^2\pi^2 - 3\lambda\mu^2 k^2\pi^2 - \lambda\sigma = 0$$

Solving this equation for λ yields the desired result. □

A first look at this equation shows that as σ grows, the location of the bifurcation becomes unbounded in λ and eventually enters negative λ space, where it is no longer physically meaningful. It also shows a result that was known from study of the Cahn-Hilliard equation, namely that the homogeneous equilibrium is globally stable if $|\mu| > \frac{\sqrt{3}}{3}$.

A second look at this equation shows that there are intersections for fixed μ, in particular that $\lambda(k, \sigma, \mu) = \lambda(j, \sigma, \mu)$ when:

$$\sigma = \frac{k^2 j^2(1 - 3\mu^2)\pi^2}{k^2 + j^2}$$

These intersections have significance. When the leftmost branch in λ for a given range of σ values passes the second-to-leftmost branch, it can be shown that the second-to-leftmost branch inherits the stability that the leftmost branch had previously. Thus these two equations together can be used to predict the boundary between the homogeneous equilibrium being stable and it being unstable. In particular, the homogeneous equilibrium is stable if:

$$\lambda < \frac{k(\sigma, \mu)^4\pi^4}{k(\sigma, \mu)^2\pi^2(1 - 3\mu^2) - \sigma} \tag{2}$$

where:

$$k(\sigma, \mu) = \min\left\{ j \in \mathbb{N} : \sigma < \frac{j^2(j+1)^2(1 - 3\mu^2)\pi^2}{j^2 + (j+1)^2} \right\} \tag{3}$$

This is consistent with findings using direct simulation, and is discussed in more detail in the next section.

This model has sufficient symmetry that by "compressing" and "reflecting" one equilibrium, one can arrive at another equilibrium at a different set of parameter values. It was shown that an $\frac{m}{n}$ fold compression and reflection of an equilibrium $u(x)$, whose dominant index (that is, twice its frequency) is divisible by n (so that the result has integer index), at parameters (λ, σ) results in a new equilibrium at parameters $(\frac{m^2\lambda}{n^2}, \frac{m^2\sigma}{n^2})$. For example, a twofold compression and reflection of $u(x)$, an equilibrium at (λ, σ, μ) would result in:

$$v(x) = \begin{cases} u(2x), x \in [0, 0.5] \\ u(2 - 2x), x \in [0.5, 1] \end{cases}$$

being an equilibrium at $(4\lambda, 4\sigma, \mu)$.

Proof. For brevity and simplicity of notation, the proof is presented only for m=2 and n=1 as in the example; the remaining cases are analogous.

Suppose u is an equilibrium of the system. That is, suppose that:

$$-u_{xxxx} - \lambda u_{xx} + \lambda(u^3)_{xx} - \lambda\sigma(u - \mu) = 0 \tag{4}$$

Then consider v(x) = u(2x) on $[0, 0.5]$. Notice that (4) is independent of space, and that the image of f(x)=2x on $[0, 0.5]$ is $[0, 1]$, where the equilibrium equation holds for u. Consequently if some function of v is exactly some function of u evaluated at a different position in $[0, 1]$, then the different evaluation position does not matter as long as it is the same across the entire expression, which it is. Thus:

$$\begin{aligned} -v_{xxxx} - 4\lambda v_{xx} + 4\lambda(v^3)_{xx} - 16\lambda\sigma(v - \mu) &=^? 0 \\ -16u_{xxxx} - 16\lambda u_{xx} + 16\lambda(u^3)_{xx} - 16\lambda\sigma(u - \mu) &=^? 0 \\ 16(-u_{xxxx} - \lambda u_{xx} + \lambda(u^3)_{xx} - \lambda\sigma(u - \mu)) &= 16 \times 0 = 0 \end{aligned}$$

as desired.

□

The proof is identical on $[0.5, 1]$, where the image of g(x)=2-2x is $[0, 1]$ again, and where the eventual factor on the outside from the chain rule is -16. The proof is essentially the same for different values of m and n, except that the number of cases increases and the factor on the outside changes.

3.2 One Parameter Continuation

One parameter continuation is used in this work to compute the bifurcation structure in λ for different σ values. This may be contrasted with two parameter continuation, discussed in Section 3.4, which is used to follow specific bifurcation points in the bifurcation diagram as σ varies.

One parameter continuation, when combined with the analytical results above, yields a conjectured bifurcation structure which is highly symmetric and highly organized. This structure is demonstrated using several example bifurcation diagrams. The first is Figure 2, which is a bifurcation diagram when $\mu = 0$ and $\sigma = 0$. This diagram, which is the bifurcation diagram for the Cahn-Hilliard equation when $\mu = 0$, is known analytically. Each branch begins at $\lambda = k^2\pi^2$; each branch has one more unstable direction than the one before it, with the first being the unique stable branch; the kth branch as λ grows is dominated by the k Fourier mode; there are no other bifurcation points.

When σ is nonzero, but small enough that the first intersection described in the analytical results has not happened, (that is, when $\sigma < \frac{4\pi^2}{5}$), the branches are still in the same order as their mode index. Near the homogeneous equilibrium, each branch still has one more unstable direction than the one before it as before, but now the jth branch has j-1 secondary bifurcation points along it, each of which removes one unstable direction until eventually stability is achieved. Thus for sufficiently large λ every branch is stable in this regime.

As σ passes $\frac{4\pi^2}{5}$ and moves on toward π^2, infinitely many intersections occur, one with each of the other branches, in order. These intersections are meaningful. As the first branch approaches the jth branch, the

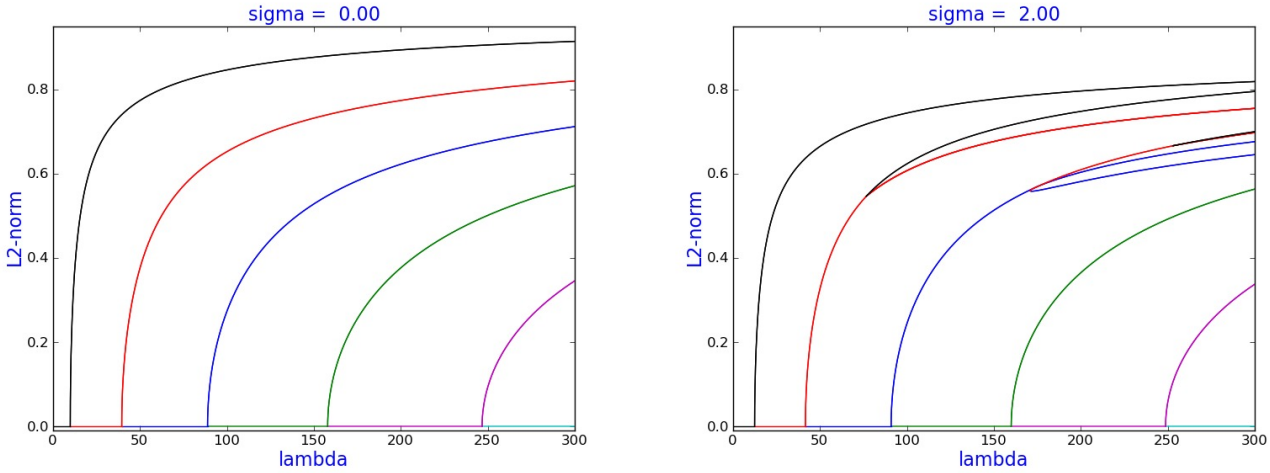

Figure 4: (a): Bifurcation diagram for $\mu = 0$, $\sigma = 0$; (b) Bifurcation diagram for $\mu = 0$, $\sigma = 2$. Observe secondary bifurcations in (b) in contrast with (a).

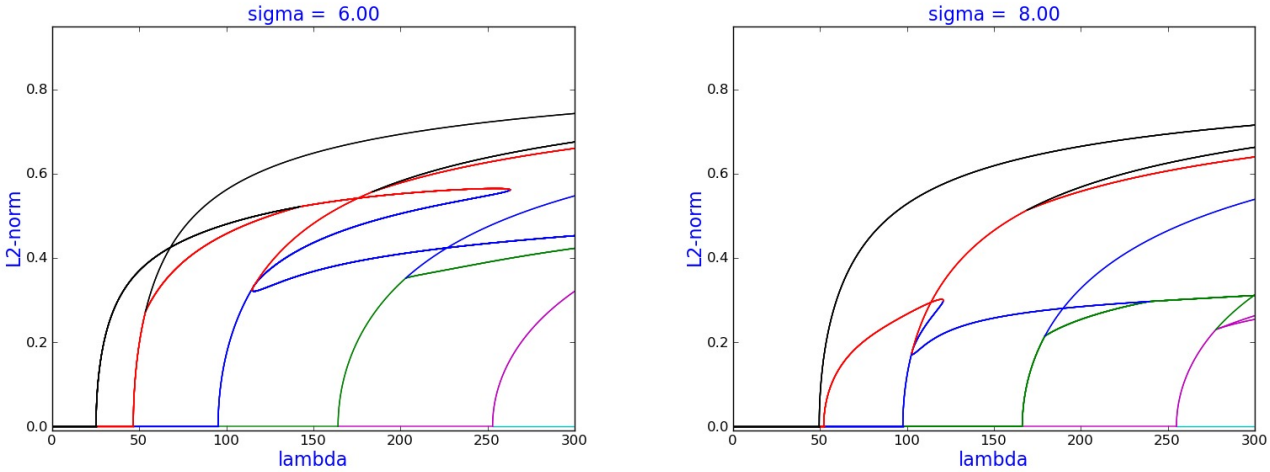

Figure 5: (a): Bifurcation diagram for $\mu = 0$, $\sigma = 6$; (b) Bifurcation diagram for $\mu = 0$, $\sigma = 8$. Observe secondary bifurcations in each case. In (b), the second branch from the left is the branch of index 1, since the first intersection has already occurred. Notice that the second branch is now stable over this entire parameter range.

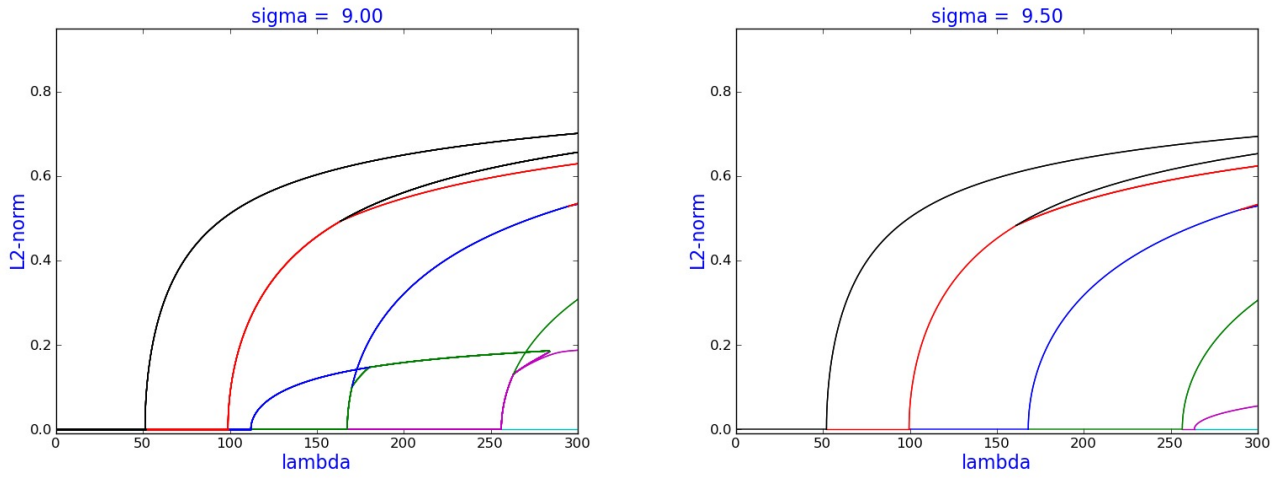

Figure 6: (a) Bifurcation diagram for $\mu = 0$, $\sigma = 9$; (b) Bifurcation diagram for $\mu = 0$, $\sigma = 9.5$. In (a), 2 intersections have occurred, and the branch of index 1 is the third from the right. In (b), 4 intersections have occurred, and the branch of index 1 is the furthest to the right. Notice that the second branch is again stable over this entire parameter range in both diagrams, and that the branches which the first branch has intersected have also lost unstable directions. .

first secondary bifurcation on the jth branch (which removes the first unstable direction of that branch) moves toward the homogeneous equilibrium, until it hits it when the two branches intersect. Afterwards, that bifurcation no longer exists, and the branch loses its unstable direction as soon as it bifurcates, passing it on to the first branch.

As the first branch intersects with all of the other branches, removing a bifurcation and an unstable direction each time, no other intersections occur until the first branch has completely disappeared. This is because:

$$\frac{2^2 3^2 \pi^2}{2^2 + 3^2} = \frac{36\pi^2}{13} > \pi^2$$

That is, the σ value where the second branch intersects the third exceeds the value where the first branch vanishes. More generally:

$$\frac{(j+1)^2(j+2)^2\pi^2}{(j+1)^2 + (j+2)^2} > j^2\pi^2$$

can be easily verified.

After this, the same pattern repeats with each branch: the branch moves off to infinity, intersects every other branch in the process, and disappears. As this proceeds, the higher modes gradually become more and more stable, until eventually when the (j-1)th branch intersects the jth branch, the jth branch becomes stable for fairly small λ. The ordering is also maintained; the second branch vanishes before the third branch intersects the fourth, etc.

The most interesting of these intersections and their corresponding secondary bifurcations are of course the ones that lead to stability. These are studied with two parameter continuation, which is discussed in Section 3.4.

3.3 Direct Simulation

Figure 7 and Figure 8 are two typical examples of the result of using direct simulation. The main difference is that with λ being larger in Figure 8, behavior similar to a higher frequency equilibrium is seen for a

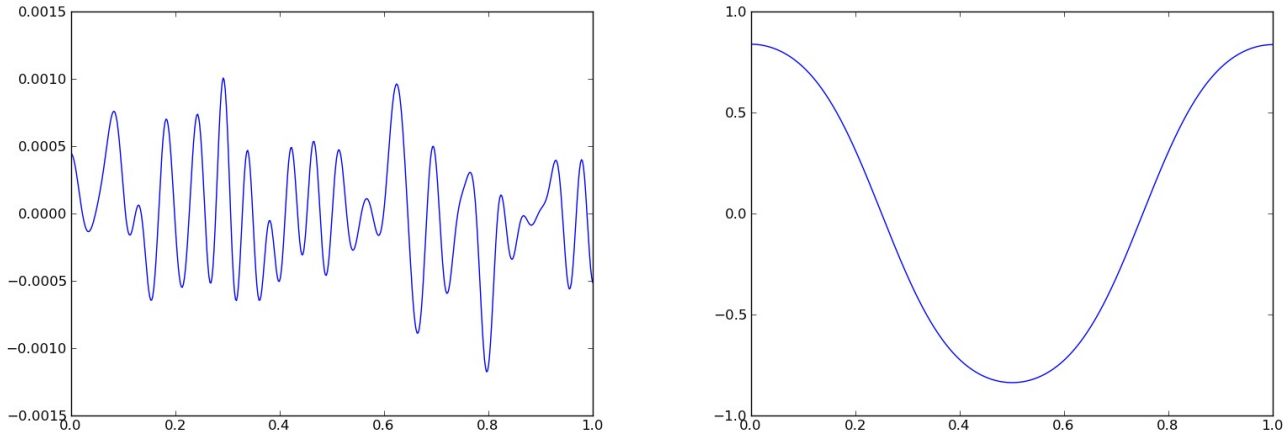

Figure 7: Simulation snapshots for $\lambda = 100$, $\sigma = 2$, $\mu = 0$. (a): The initial condition is a random perturbation of the homogeneous equilibrium. (b): Within 0.01 time units the solution has appeared to converge to its long term state.

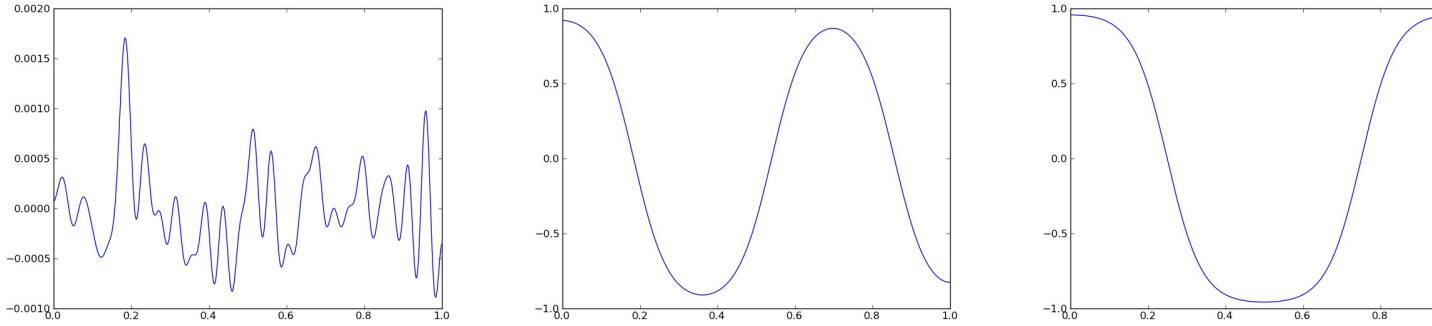

Figure 8: Simulation snapshots for $\lambda = 260$, $\sigma = 2$, $\mu = 0$. (a) The initial condition is again a random pertubation of the homogeneous equilibrium. (b) The state after 0.01 time units is a mode 3 type solution, which equilibrium methods would predict to be unstable. (c) Within 0.1 time units the apparent long term state of a mode 2 type solution appears.

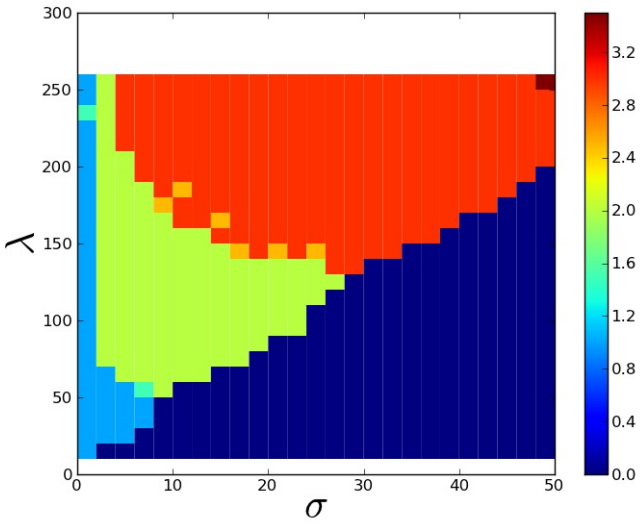

Figure 9: Diagram computed using direct simulation. Colors denote mode stabilities; dark blue denotes the homogeneous equilibrium is stable, teal denotes the mode 1 solution is stable etc., intermediate colors denote (apparent) multistability.

significant amount of time before the stable lower frequency solution emerges, while in Figure 7 the lower frequency equilibrium is seen within less than 0.01 time units. This behavior with increasing λ is typical.

The main result derived from direct simulation is the simulation diagram Figure 9. This diagram plots the long-term dominant mode in simulations over a grid in the (σ, λ) plane. It is a very coarse diagram, with jagged edges, but it demonstrates some general patterns. First, as σ increases, lower modes become less and less stable until eventually the homogeneous equilibrium becomes globally stable. The latter result is proven analytically above. Second, as λ increases, higher modes become more and more stable in general; however, if σ is kept small, this does not give the entire picture. In particular, it is known from study of the Cahn-Hilliard equation (equivalent to the diblock copolymer equation with $\sigma = 0$) that the unique stable equilibrium is the mode 1 equilibrium when $\lambda > \frac{\pi^2}{1-3\mu^2}$ and $|\mu| < \frac{\sqrt{3}}{3}$. In addition, as λ is increased while σ is held fixed, the extent to which λ must rise to reach a new mode is quite considerable, relative to increasing σ and λ together.

3.4 Two Parameter Continuation

In performing one parameter continuation with stability computation, it was found that a specific bifurcation exists which stabilizes a given branch. Moreover, it was found using direct simulation that when λ exceeds the λ value at this bifurcation, the newly stabilized branch is often reached over time, even if other stable solutions exist.

Thus it was found that this bifurcation is central to the long-term behavior of the model. In particular, if its location in (σ, λ) space could be tracked, then the boundary between different long-term behaviors could be determined, creating a phase diagram. This can be done using two parameter continuation of bifurcation points, which is implemented in AUTO. In this method, the initial point is a bifurcation point for a given set of parameter values, and the method then proceeds to find bifurcation points at other parameter values. A partial phase diagram is depicted in Figure 10.

This diagram gives a relatively full picture of the long-term behavior of the model, with smooth separations between the regions. It is analogous to Figure 9, made using direct simulation, but was constructed using numerical continuation, without which the smooth separation between regions are not possible. The

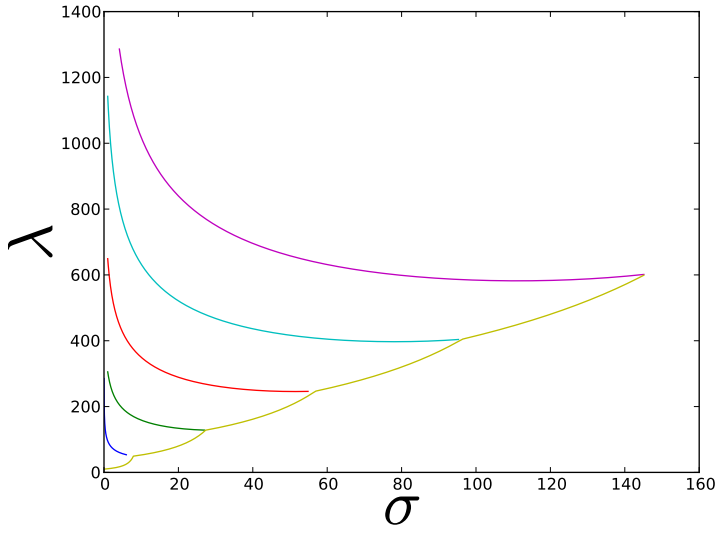

Figure 10: A "phase diagram" depicting mode stability as a function of λ and σ with $\mu = 0$. The bottom right region has the homogeneous equilibrium being stable; the other regions have modes 1, 2, and 3 being stable, with the index growing with λ and σ. The bottom curve is analytical, being the equality form of (2), with the cusps being the points at which k changes value as per (3). The remaining curves are numerical.

picture given by this diagram is only relatively full because it does not indicate instability boundaries and because it does not say anything about basins of attraction of the stable equilibria. The former issue can in principle be corrected using numerical continuation of destabilizing bifurcation points. This has been attempted, however it is much more difficult numerically than following the stabilizing bifurcation points because the λ value grows very rapidly as the σ value decreases. Since λ is the coefficient of the nonlinearity, this means that the equation rapidly becomes "more nonlinear" and consequently more and more Fourier modes become necessary to achieve convergence.

The construction of this diagram was performed by making σ slightly less than $\frac{j^2(j+1)^2\pi^2}{j^2+(j+1)^2}$ for each branch $j = 2, \ldots, 6$. Then the stabilizing bifurcation exists but is also close to the homogeneous equilibrium, making it easy to obtain by one parameter continuation. Then the position of the bifurcation point is continued in two parameters; this method is built directly into AUTO.

3.5 Intermittency

With the phase diagram in hand, the question of how the system changes as a boundary is approached and eventually passed can be asked. This question can be answered using direct simulation. Performing direct simulation near the $1 \to 2$ boundary (the dark blue curve in Figure 10) reveals the phenomenon of **intermittency**. Intermittency occurs when a branch is soon to become stable but is not yet stable. It is characterized by the solutions on this weakly unstable branch appearing for a long time in the dynamics before the system eventually moves towards the actual stable solution.

In performing simulations near the $1 \to 2$ boundary from below as exemplified in Figure 11, it was found that the mode 2 structure appears intermittently before the mode 1 structure eventually appears. Getting closer to the boundary increases the time needed for the stable structure to appear. This suggests that attempting to construct this phase diagram by direct simulation would have proved difficult, because very close to the boundary very long simulations would have been necessary to be sure that the mode 2 structure was already stable.

This intermittency also describes how the mode 1 solution disappears from the long-term dynamics before

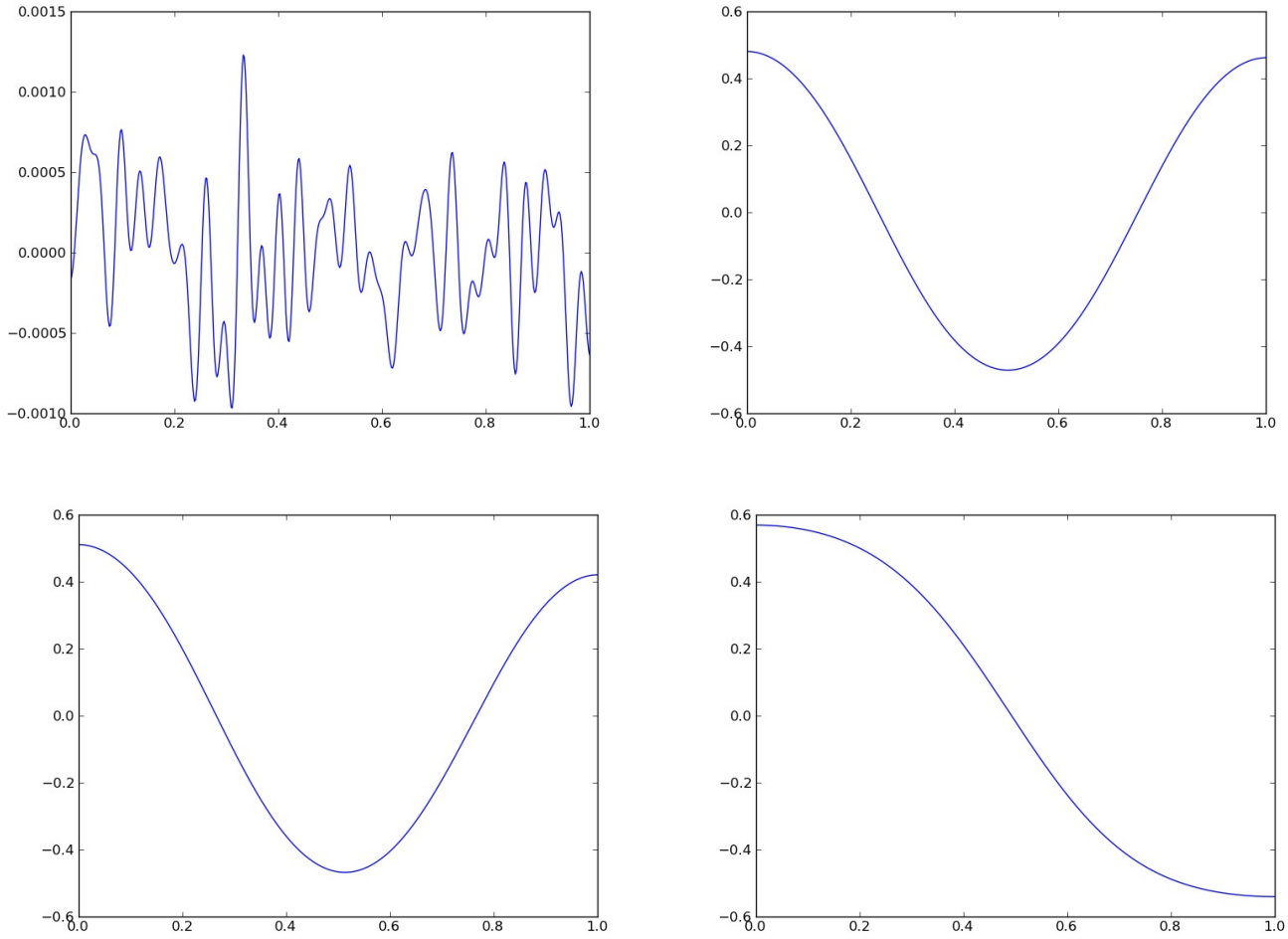

Figure 11: Simulation snapshots for $\lambda = 56$, $\sigma = 5$, $\mu = 0$. (a): The initial condition. (b) The state after 0.1 time units. The state resembles a mode 2 type state. (c) The state after 0.3 time units. The state still closely resembles a mode 2 type state, however the symmetry is clearly broken, with the right side being distinctly lower than the left. (d) The apparent long term state, reached after 0.4 time units, is of mode 1 type, as expected by stability computation.

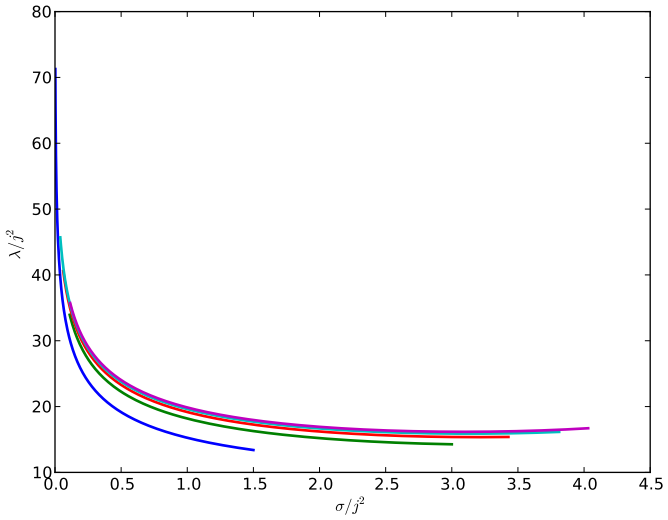

Figure 12: A scaled version of the two parameter phase diagram from Figure 10, using the scaling in (**??**). The right endpoints were shown to converge with this scaling; the numerics suggest that the entire curves may also converge with this scaling. Each point can be interpreted as an equilibrium on the first branch.

it becomes unstable. It seems that even before the mode 2 branch is stable, a random perturbation leads the system into its domain of attraction, and so the system stays there until it eventually gets close enough for the instability of the equilibrium to send it away. After the second branch is already stable, the system is still being led into its domain of attraction from random perturbations. Thus the system, being in the domain of attraction of a stable equilibrium, converges to that equilibrium, even though there is another stable equilibrium available.

This result may seem to call the multistability result from stability computation into question to some extent. In short, if the first branch is not unstable, why is it not present in long-term dynamics? It turns out that it is present, but that reaching it instead of being brought towards the second branch is "difficult". However, with the correct initial conditions, in this case perturbing in the eigendirection corresponding to the first branch, simulations show that it is in fact reached. Thus, rather than being absent from the dynamics, the first branch takes on a domain of attraction which does not include "typical" perturbations from the homogeneous equilibrium.

3.6 Asymptotic Analysis

It would be desirable to have some sort of asymptotic characterization of the full form of Figure 10. The most obvious guess would be to say that the points on branch 2j are simply j-fold compressions and reflections of a point on branch 2, which would mean that a point (σ_j, λ_j) on branch j would simply correspond to $\frac{j^2}{4}(\sigma, \lambda)$ for a point (σ, λ) on branch 2. Indeed, such a point not only would be another equilibrium point, but is also another bifurcation point; the bifurcation equation has sufficient symmetry for this as well. Moreover, this kind of intuition is correct in the Cahn-Hilliard equation: every non-monotone equilibrium (that is, every equilibrium not on the first branch) is a compression and reflection of a monotone equilibrium in the Cahn-Hilliard equation.

However, this new point is not actually the point which stabilizes branch j. The bifurcation which stabilizes branch j can be intuitively thought of as being related to the intersection between branch j-1 and branch j. That is, as branch j-1 intersects branch j, that bifurcation vanishes, and so if σ is somewhat smaller than needed to obtain the intersection, that bifurcation exists and is very close to the homogeneous

equilibrium, making it the only bifurcation which adds stability to branch j.

The issue here, then, is that when the entire space is shifted, say by doubling every branch index, now branches 2j-2 and 2j are the next ones to intersect, and so the first bifurcation on branch 2j is the one which removes its second-to-last unstable direction. It has been shown that this first bifurcation on branch kj is the one that is found when branch j is scaled by a factor of k^2, which means that this scaling alone will not find the exact location of the bifurcation stabilizing branch 2j. And indeed, it is clear that there is no way to scale branch 2j-1 and 2j down to smaller indices together.

However, both parameters of the intersection points of the two parameter curves with the homogeneous equilibrium (the right endpoints of the curves in Figure 10) are asymptotically quadratic in the index.

Proof:

The intersection of index j ($j \geq 2$) occurs at:

$$(\sigma, \lambda) = \left(\frac{j^2(j-1)^2(1-3\mu^2)\pi^2}{j^2+(j-1)^2}, \frac{j^4\pi^4}{j^2\pi^2(1-3\mu^2)-\sigma} \right)$$

which, substituting the expression for σ, results in:

$$(\sigma, \lambda) = \left(\frac{j^2(j-1)^2(1-3\mu^2)\pi^2}{j^2+(j-1)^2}, \frac{j^4\pi^4}{j^2\pi^2(1-3\mu^2)-\frac{j^2(j-1)^2(1-3\mu^2)\pi^2}{j^2+(j-1)^2}} \right)$$

Simplification in the λ expression results in:

$$(\sigma, \lambda) = \left(\frac{j^2(j-1)^2\pi^2(1-3\mu^2)}{j^2+(j-1)^2}, \frac{\pi^2(j^2+(j-1)^2)}{1-3\mu^2} \right)$$

Scaling by j^2 yields:

$$\left(\frac{\sigma}{j^2}, \frac{\lambda}{j^2} \right) = \left(\frac{(j-1)^2\pi^2(1-3\mu^2)}{j^2+(j-1)^2}, \frac{\pi^2(j^2+(j-1)^2)}{j^2(1-3\mu^2)} \right)$$

which converges to $(\frac{\pi^2(1-3\mu^2)}{2}, \frac{2\pi^2}{1-3\mu^2})$ as $j \to \infty$.

Scaling by j^2 is essentially equivalent to finding the equilibrium on the first branch which corresponds to each equilibrium. At the homogeneous equilibrium itself, which is where the preceding argument is relevant, the scaling is insignificant; the homogeneous equilibrium exists for all parameter values. However, if the entire two parameter branch is scaled in this way, a collection of equilibria on the first branch are obtained. Performing this procedure on the two parameter curves with $\mu = 0$ yields a sequence of curves which seem to converge everywhere. Figure 12 shows the first five of these scaled curves. If this sequence does, in fact, converge everywhere, then the structure of the full phase diagram can be arbitrarily approximated by numerically computing a collection of curves and then scaling them as needed.

4 Conclusion

The partial bifurcation structure for the diblock copolymer equation in one dimension was computed using the software package AUTO. The conjectured full bifurcation structure consists of a family of diagrams, parametrized by σ. The conjectured impact of σ on the bifurcation structure is quite regular. In summary:

For $\sigma = 0$, all branches j have j-1 unstable directions. For every nonzero σ, j-1 secondary bifurcations exist on every branch j, each removing an unstable direction from that branch. The secondary curves associated with these bifurcations intersect the first branch, at which point the first branch takes on their unstable direction. As σ grows, these bifurcations move backward in λ and thus closer to the homogeneous equilibrium. At the same time, the first branch moves outward intersecting all the other branches, and when it intersects a branch, the first bifurcation on that branch disappears, globally removing an unstable direction. The first branch disappears for $\sigma > \pi^2$ and then the process repeats.

A standard approach using direct simulation to determine long-term behavior was performed, resulting in a coarse stability diagram with some metastability problems, including a point where the Cahn-Hilliard case did not converge to the monotone solution on the time scale used. Using the bifurcation structure just described, a two parameter "phase diagram" was constructed. This diagram is much smoother, and because it based on equilibrium behavior, there is no concern about metastability influencing the results. However, it only depicts what long-term behaviors are possible; where multistability exists it says nothing about the attractor structure of the different stable equilibria.

5 References

[1] F.S. Bates and G. H. Fredrickson, *Block Copolymers - Designer Soft Materials*, Physics Today **52** (1999), 32-38.

[2] ———, *Block Copolymer Thermodynamics: Theory and Experiment*, Annual Review of Physical Chemistry **41** (1990), 525-57.

[3] R. Choksi, M. A. Peletier, and J. F. Williams, *On the Phase Diagram for Microphase Separation of Diblock Copolymers: an Approach via a Nonlocal Cahn-Hilliard Functional*, SIAM Journal on Applied Mathematics **69** (2009), 1712-38.

[4] R. Choksi and X. Ren, *On the Derivation of a Density Functional Theory for Microphase Separation of Diblock Copolymers*, Journal of Statistical Physics **113** (2003), 151-76.

[5] M. Grinfeld and A. Novick-Cohen, *Counting stationary solutions of the Cahn-Hilliard equation by transversality arguments*, Proceedings of the Royal Society of Edinburgh **125A** (1995), 351-370.